

Supplementary Information: Point-defect chemistry for ionic conduction in solid electrolytes with isovalent cation mixing

Takafumi Ogawa,^{*a} Kazuyuki Sato,^b Kazuhiro Mori,^c Shunsuke Kobayashi,^a Hiroki Moriwake,^a Yuichi Ikuhara,^{d,a} and Akihide Kuwabara^a

1 Lattice constants from NPT-ensemble MD simulations

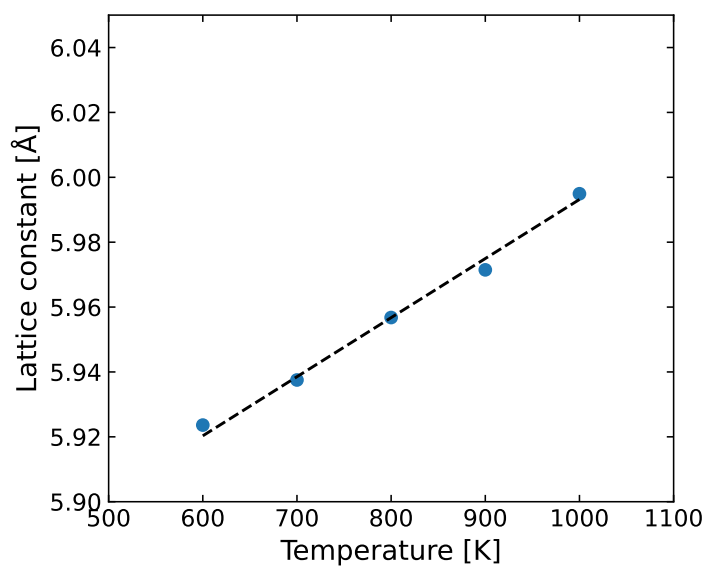


Fig. S1 Lattice constant as a function of temperature for $\text{Ba}_{0.5}\text{Ca}_{0.5}\text{F}_2$, from NPT-ensemble MD simulations with the trained MLFF. The trend is fitted by using the equation $l(T) = 5.811 + 1.8213 \times 10^{-4}T$, which is shown in a black dashed line.

^a Nanostructures Research Laboratory, Japan Fine Ceramics Center, Nagoya 456-8587, Japan.

^b Office of Society-Academia Collaboration for Innovation, Kyoto University, Uji, Kyoto 611-0011, Japan.

^c Institute of Materials Structure Science, High Energy Accelerator Research Organization (KEK), Ibaraki 319-1106, Japan.

^d Institute of Engineering Innovation, The University of Tokyo, Tokyo 113-8656, Japan.

* E-mail: t_ogawa@jfcc.or.jp.

2 Recheck of MLFF accuracy

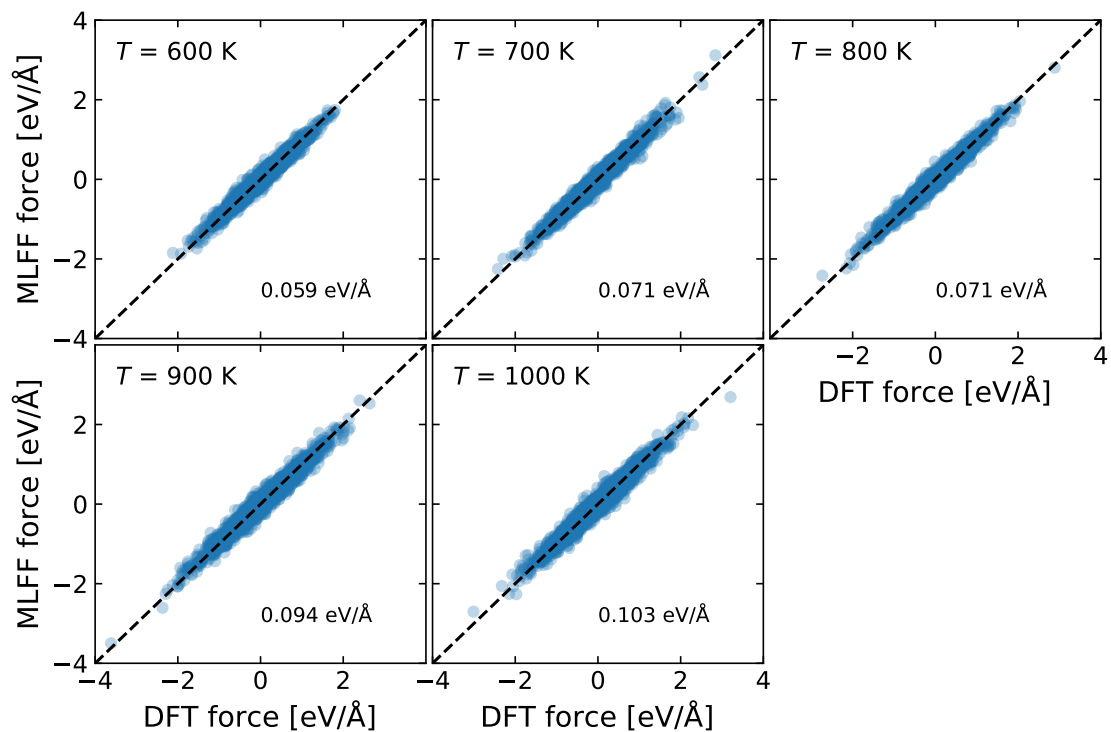


Fig. S2 Correlation plot between MLFF and DFT forces for snapshot structures of $\text{Ba}_{0.5}\text{Ca}_{0.5}\text{F}_2$ from sampling MD simulations with the larger cell. The root mean square error (RMSE) value is written in each panel. The linear correlation is well retained. The RMSE values are slightly larger than the values in the learning step, but are within an admissible range of high-temperature simulations.¹ In addition, the differences in energies and stresses between MLFF and DFT are comparable to the RMSE values in the learning step.

3 Difference in the defect formation energy

In this section, the details for calculating the difference in defect formation energy were summarized. Defect formation energy, E_{def} , of defect D^q with charge q , is defined as follows:^{2,3}

$$E_{\text{def}}(D^q) = E(D^q) - E^0 + \Delta E_c(D^q) - \sum_{\alpha} \Delta n_{\alpha}(D^q) \mu_{\alpha} + q \mu_e, \quad (\text{S1})$$

where $E(D^q)$ and E^0 are the DFT energies for supercells with and without the defect, respectively, and $\Delta n_{\alpha}(D^q)$ is the difference in the number of α atom caused by defect formation. $\Delta E_c(D^q)$ means correction term as described in the main text. μ_{α} and μ_e are the chemical potentials of α atom and an electron, respectively. In this work, the potential of an F atom (μ_{F}) is taken as a variable parameter ranging between the limit values determined by the reactions, Li/LiF and Cu/CuF₂ (Fig. S4), whereas μ_e is defined in each compound via the charge neutrality condition. μ_e in compound C is explicitly denoted as μ_e^C . The difference in the formation energy of D^q between compound C and BaF₂ is derived as follows:

$$\begin{aligned} E_{\text{def}}^C(D^q) - E_{\text{def}}^{\text{BaF}_2}(D^q) &= \{E^C(D^q) - E^{C,0} + \Delta E_c^C(D^q)\} - \{E^{\text{BaF}_2}(D^q) - E^{\text{BaF}_2,0} + \Delta E_c^{\text{BaF}_2}(D^q)\} \\ &\quad + q(\mu_e^C - \mu_e^{\text{BaF}_2}). \end{aligned} \quad (\text{S2})$$

In executing the last term, μ_e^C is replaced by the expression with the valence band maximum energy, E_{VBM}^C , and Fermi level, ϵ_{F}^C , thereby obtaining the following equation:

$$\mu_e^C - \mu_e^{\text{BaF}_2} = (\epsilon_{\text{F}}^C + E_{\text{VBM}}^C) - (\epsilon_{\text{F}}^{\text{BaF}_2} + E_{\text{VBM}}^{\text{BaF}_2}). \quad (\text{S3})$$

In measuring the Fermi level position on an equal footing, the valence band offset between the two compounds, $\Delta V_{\text{offset}}^{C|\text{BaF}_2}$, was considered. The offset is defined as follows:⁴

$$\Delta V_{\text{offset}}^{C|\text{BaF}_2} = (E_{\text{VBM}}^C - \bar{V}_{\text{Bulk}}^C) - (E_{\text{VBM}}^{\text{BaF}_2} - \bar{V}_{\text{Bulk}}^{\text{BaF}_2}) + (\bar{V}_{\text{Het}}^C[C|\text{BaF}_2] - \bar{V}_{\text{Het}}^{\text{BaF}_2}[C|\text{BaF}_2]), \quad (\text{S4})$$

where \bar{V}_{Bulk}^C and $\bar{V}_{\text{Het}}^C[C|\text{BaF}_2]$ are the reference energies for the bulk system and the bulk-like region in the heterostructure, including alternating C and BaF₂ slabs, respectively. As the reference energies, an averaged electrostatic potential was observed rather than core-level potentials.⁴ By replacing E_{VBM}^C in Eq. (S3) by using Eq. (S4), the difference in chemical potentials is rewritten as follows:

$$\begin{aligned} \mu_e^C - \mu_e^{\text{BaF}_2} &= (\epsilon_{\text{F}}^C + E_{\text{VBM}}^{\text{BaF}_2} + \Delta V_{\text{offset}}^{C|\text{BaF}_2}) - (\epsilon_{\text{F}}^{\text{BaF}_2} + E_{\text{VBM}}^{\text{BaF}_2}) \\ &\quad + (\bar{V}_{\text{Bulk}}^C - \bar{V}_{\text{Bulk}}^{\text{BaF}_2}) - (\bar{V}_{\text{Het}}^C[C|\text{BaF}_2] - \bar{V}_{\text{Het}}^{\text{BaF}_2}[C|\text{BaF}_2]). \end{aligned} \quad (\text{S5})$$

The first parenthesis term in the right hand side in this equation corresponds to the Fermi level measured from the valence band maximum of BaF₂. The second term is cancelled by the first term when considering point-defect stability in the heterostructure system. Therefore, the target energy difference can be obtained by calculating the reference energies in the third and fourth terms shown in Eq. (S5).

The required reference energies (the series of \bar{V}) were calculated using the same procedure as previous literature.^{4,5} In this work, heterostructures were constructed to include over eight conventional units of the fluorite structure in each slab, and the lattice constants in directions perpendicular to the interfaces were set to the averaged value between the two phases. The cell parameter in the z direction along the alternating staking and internal atom positions were optimized. Consequently, slight values were obtained for all \bar{V}_{Bulk}^C and $(\bar{V}_{\text{Het}}^C[C|\text{BaF}_2] - \bar{V}_{\text{Het}}^{\text{BaF}_2}[C|\text{BaF}_2])$ except for two types of combinations, including CdF₂|BaF₂ and PbF₂|BaF₂. The structure model and electrostatic potential for PbF₂|BaF₂ heterostructure are shown in Fig. S3 as an example. From the difference in the flat average values in the figure, $(\bar{V}_{\text{Het}}^{\text{PbF}_2}[\text{PbF}_2|\text{BaF}_2] - \bar{V}_{\text{Het}}^{\text{BaF}_2}[\text{PbF}_2|\text{BaF}_2])$ value is -2.33 eV, whereas CdF₂|BaF₂ is 0.69 eV. These energy offsets certainly affect the diagram of point-defect stability plotted in Fig. 9 of the main text.

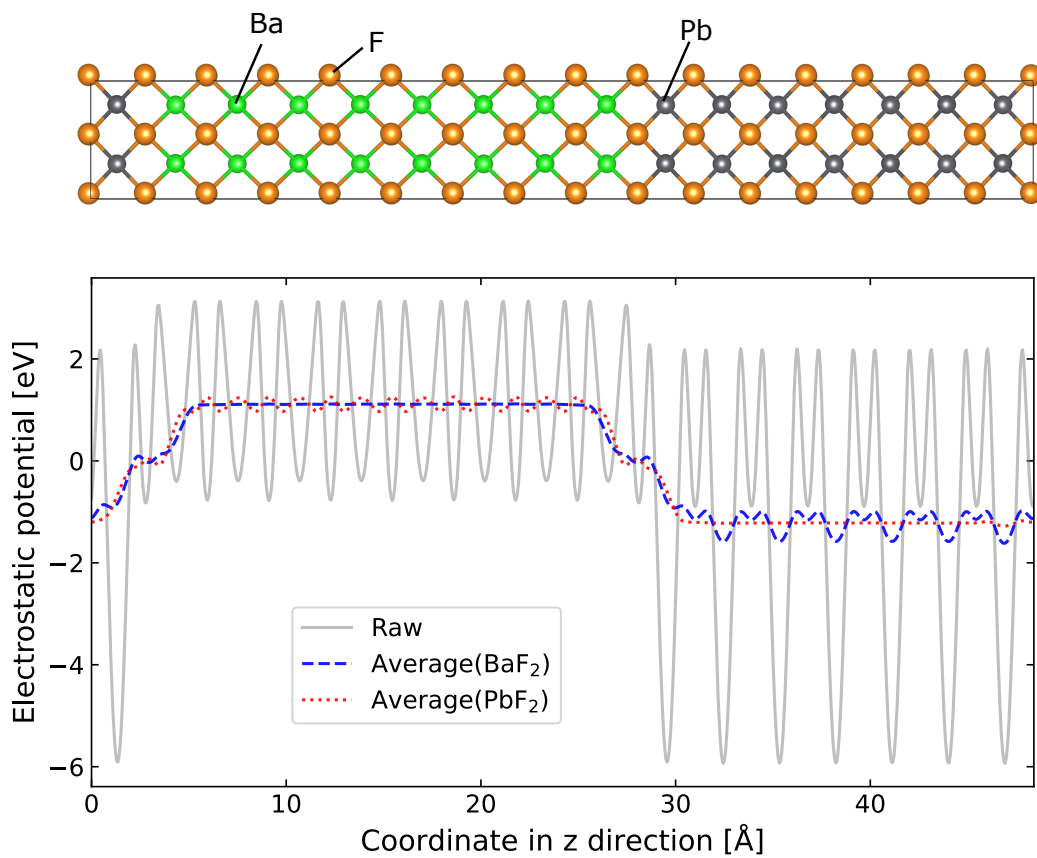


Fig. S3 Structure model and calculated electrostatic potential for the $\text{PbF}_2|\text{BaF}_2$ heterostructure. The potentials are averaged along the z -direction with the repetition units in each phase.

4 Equilibrium μ_F calculations

Equilibrium F-atom chemical potentials for various metal/metal-fluorides (M/MF_n) are listed in Fig. S4. In DFT calculations, the same conditions as in the main calculations were used, but the DFT+ U method was adopted for transition metals and Ce atom within the Dudarev's formalism.⁶ Although the U values for the $3d$ orbital of transition metals were taken from the literature,⁷ the U value for the $4f$ orbital of Ce was set to 3.0 eV in accordance with the data of cerium oxides.⁸ As shown in the figure, a theoretical open-circuit voltage can be extracted between two different electrode materials, and the theoretical relative stability of a metal fluoride in (all-solid-state) fluoride-ion batteries can be assessed.⁹⁻¹¹

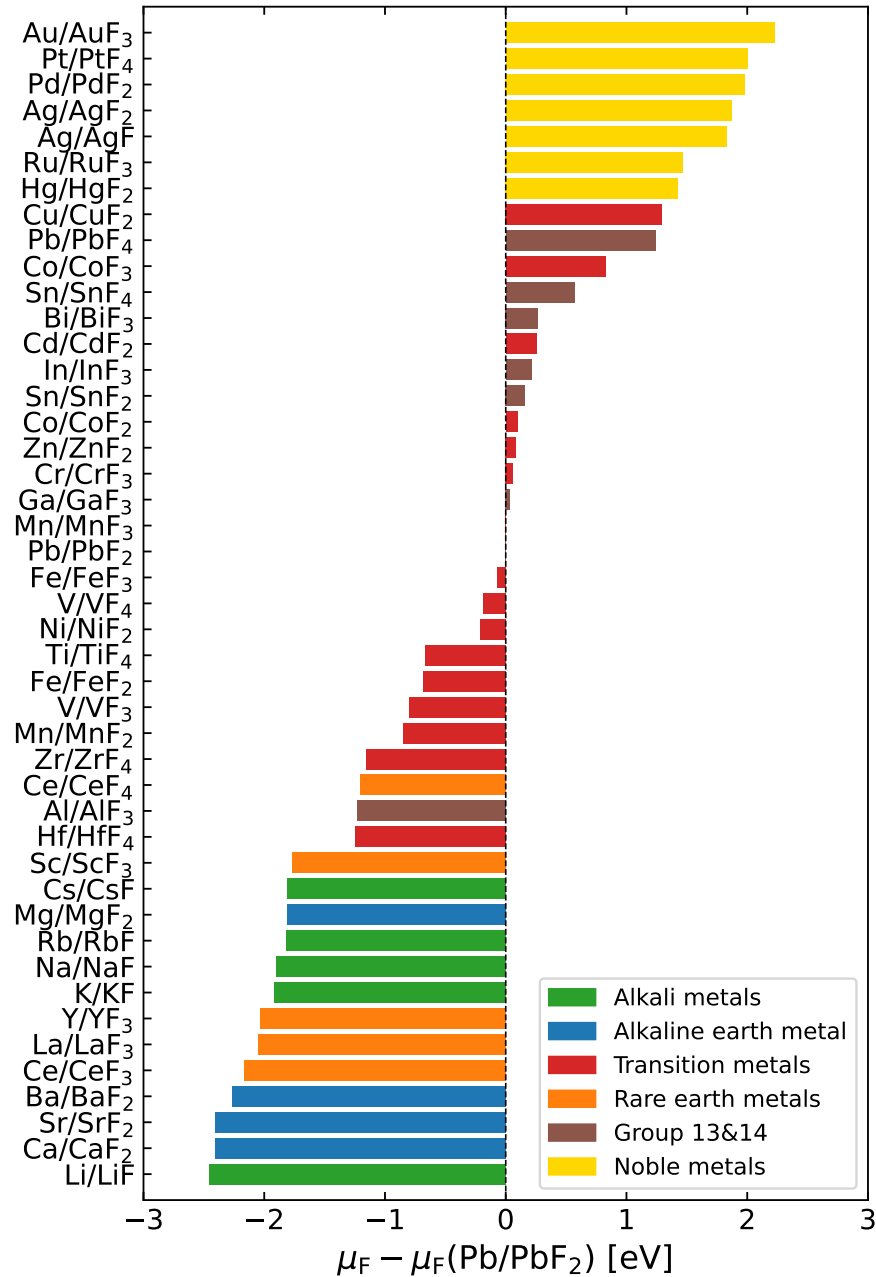


Fig. S4 Equilibrium chemical potential of fluorine atoms, μ_F , for selected M/MF_n reactions. The melting points of the fluorides are above 200 °C. The origin is set to the value for Pb/PbF₂.

5 Electronic-structure analysis of AF_2

Table S1 Summary of Löwdin charges, $Q_{\text{Löwdin}}$, and Madelung energy, E_{Madelung} , for AF_2 .

Compound	R_{ion}	$Q_{\text{Löwdin}}(A)$ [e]	$Q_{\text{Löwdin}}(F)$ [e]	E_{Madelung} [eV]
CdF ₂	1.10	1.50	-0.75	-67.0
CaF ₂	1.12	1.64	-0.82	-82.6
SrF ₂	1.26	1.68	-0.84	-82.1
PbF ₂	1.29	1.03	-0.52	-30.2
BaF ₂	1.42	1.73	-0.87	-81.1

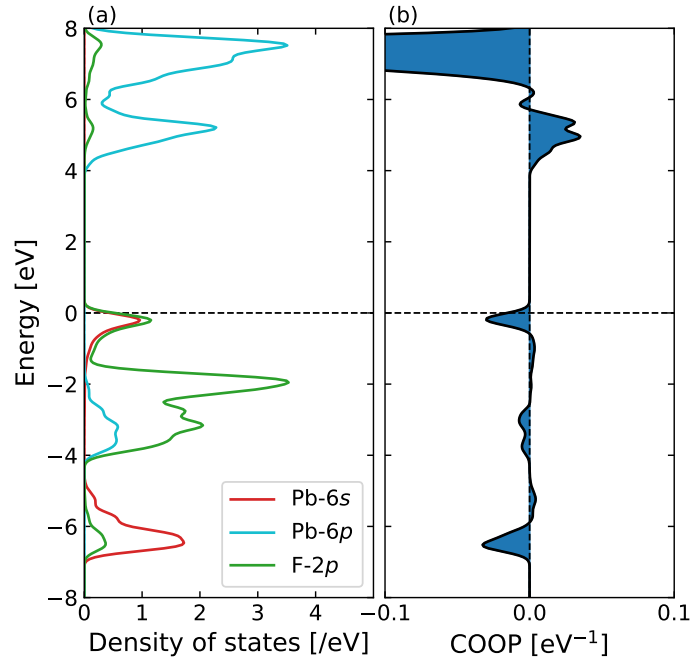


Fig. S5 (a) Density of states and (b) COOP between neighboring Pb and F atoms in PbF_2 . The valence band exhibits antibonding hybridization between Pb 6s and F 2p orbitals as well as hybridization between Pb 6p and F 2p orbitals, which are similar to other lead compounds.¹²⁻¹⁴

6 Local structures of the interstitial F atoms

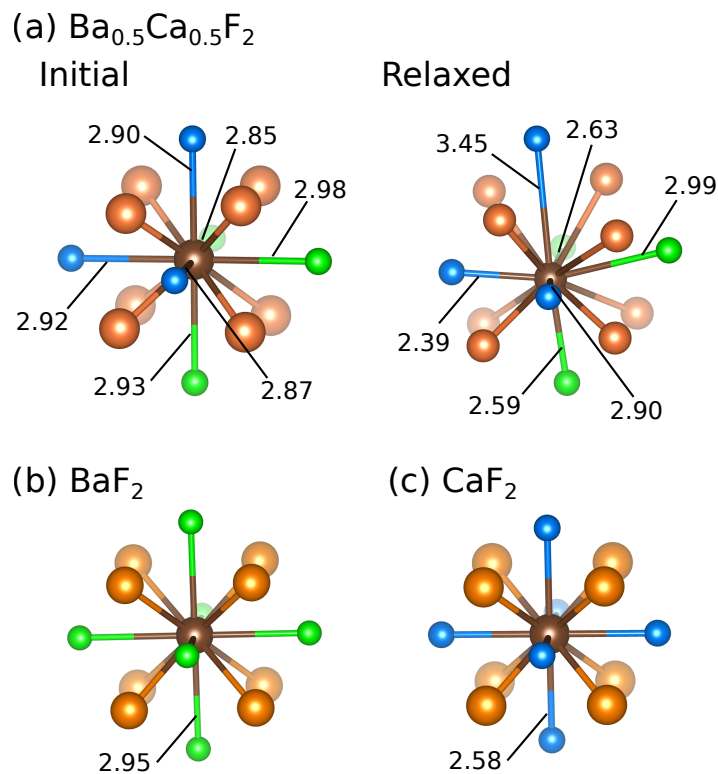


Fig. S6 The local structure of interstitial F atoms (F_{int}^i) in (a) $\text{Ba}_{0.5}\text{Ca}_{0.5}\text{F}_2$, (b) BaF_2 , and (c) CaF_2 . For $\text{Ba}_{0.5}\text{Ca}_{0.5}\text{F}_2$ (a), the defect with the lowest energy is selected as an example, and the structure before relaxation is also shown. The brown spheres at the center represent the interstitial F atoms, while the green, blue, and orange spheres represent neighboring Ba, Ca, F atoms, respectively. Bond lengths between the interstitial atom and neighboring cations are shown in the unit of \AA . Other F_{int}^i in $\text{Ba}_{0.5}\text{Ca}_{0.5}\text{F}_2$ also have similar local distortions after relaxation. For the cases of BaF_2 (b) and CaF_2 (c), the six bond lengths between the interstitial F atom and the neighboring cations in the relaxed structures are nearly identical.

References

- 1 R. Jinnouchi, J. Lahnsteiner, F. Karsai, G. Kresse and M. Bokdam, *Phys. Rev. Lett.*, 2019, **122**, 225701.
- 2 C. Freysoldt, B. Grabowski, T. Hickel, J. Neugebauer, G. Kresse, A. Janotti and C. G. Van de Walle, *Rev. Mod. Phys.*, 2014, **86**, 253–305.
- 3 T. Ogawa, A. Taguchi and A. Kuwabara, *npj Comput. Mater.*, 2022, **8**, 79.
- 4 G. D. Liberto and G. Pacchioni, *J. Phys.: Condens. Matter*, 2021, **33**, 415002.
- 5 N. R. D’Amico, G. Cantele and D. Ninno, *Appl. Phys. Lett.*, 2012, **101**, 141606.
- 6 S. L. Dudarev, G. A. Botton, S. Y. Savrasov, C. J. Humphreys and A. P. Sutton, *Phys. Rev. B*, 1998, **57**, 1505.
- 7 A. Wang, R. Kingsbury, M. McDermott, M. Horton, A. Jain, S. P. Ong, S. Dwaraknath and K. A. Persson, *Sci. Rep.*, 2021, **11**, 15496.
- 8 C. Loschen, J. Carrasco, K. M. Neyman and F. Illas, *Phys. Rev. B*, 2007, **75**, 035115.
- 9 K. Motohashi, T. Nakamura, Y. Kimura, Y. Uchimoto and K. Amezawa, *Solid State Ionics*, 2019, **338**, 113–120.
- 10 D. Zhang, K. Yamamoto, A. Ochi, Y. Wang, T. Yoshinari, K. Nakanishi, H. Nakano, H. Miki, S. Nakanishi, H. Iba, T. Uchiyama, T. Watanabe, K. Amezawa and Y. Uchimoto, *J. Mater. Chem. A*, 2021, **9**, 406–412.
- 11 F. Gschwind, G. Rodriguez-Garcia, D. J. S. Sandbeck, A. Gross, M. Weil, M. Fichtner and N. Hörmann, *J. Fluorine Chem.*, 2016, **182**, 76–90.
- 12 G. Trinquier and R. Hoffmann, *J. Phys. Chem.*, 1984, **88**, 6696–6711.
- 13 A. Walsh and G. W. Watson, *J. Solid State Chem.*, 2005, **178**, 1422–1428.
- 14 M. G. Goesten and R. Hoffmann, *J. Am. Chem. Soc.*, 2018, **140**, 12996–13010.